Article

Application of Multi-Cylinder Synchronous Control for Telescopic Mechanism of Marine Steel Pile Cleaning Equipment

Chao Li [1], Nan Pang [2,*], Kai Xu [3,*], Qingling Geng [1], Xiangyu Wang [4], Feihong Yun [5] and Lei Gao [6]

1   Guangdong Mechanical and Electronical College of Technology, Guangzhou 510515, China
2   College of Mechanical and Electrical Engineering, Guilin University of Aerospace Technology, Guilin 541004, China
3   Wuhan Institute of Shipbuilding Technology, Wuhan 430212, China
4   Yantai Research Institute of Harbin Engineering University, Yantai 264006, China
5   College of Mechanical and Electrical Engineering, Harbin Engineering University, Harbin 150001, China
6   School of Economics and Management, Yanshan University, Qinhuangdao 066004, China
*   Correspondence: 435818875@hrbeu.edu.cn (N.P.); xukai0705@163.com (K.X.)

Abstract: In order to clean up marine fouling attached to marine steel pile, this paper proposed an innovative configuration scheme of the marine steel pile cleaning equipment by the scraping method and its telescopic mechanism by applying a multi-cylinder synchronous control strategy to the cleaning equipment, and produced a test prototype of the cleaning equipment that could solve the problem of cleaning equipment eccentricity and tilt in the field of ocean engineering. Based on the MATLAB Simulink module, a simulation model of the operation process of the telescopic mechanism of the marine steel pile cleaning equipment was established to complete the evaluation of the multi-cylinder synchronous control performance under multiple working conditions. Through the test, the synchronous working performance of the telescopic mechanism of the cleaning equipment under the no-load condition was preliminarily verified. The test results showed that under the no-load condition, the relative errors between the three cylinders and the target displacement were 0.8%, 0.4%, and 0.2%, respectively, and the cleaning equipment could reach the specified working position at the given working speed. The displacement synchronization error between each cylinder was 0.7 mm, 0.7 mm, and 0.6 mm, respectively, and the displacement synchronization error was controlled within 1 mm. The telescopic mechanism had good synchronization, which can ensure the stability and prevent the eccentricity and tilt during the cleaning equipment operation as well as provide a valuable reference for the manufacturing of cleaning equipment.

Keywords: marine steel pile; cleaning equipment; telescopic mechanism; synchronous control; Simulink simulation; test

1. Introduction

With the development and utilization of marine resources, a large number of marine infrastructures have been built. Among them, a large number of metal materials have been used for marine steel piles [1]. Most of the marine steel piles standing in the ocean have been corroded by attached fouling organisms including thousands of species [2]. The corrosion pattern of marine steel piles in different marine environmental zones is different, and the wave splash zone is more severely affected by fouling organism attachment and corrosion [3,4]. Because of its special location, these steel structures are affected by many factors, for example, alternating cycles of drying and wetting of the salt film, salt enrichment, sunlight, spray impact, fouling organisms attachment, etc. [5], of which the attachment corrosion of fouling organisms is particularly serious [6]. Over time, a solid, rough, thick crust will form, which can increase the surface area of the steel pile and the resistance it experiences in seawater [7], thus increasing its surface corrosion and reducing its service life [8,9]. The corrosion rate in the wave splash zone is about 3 to 10 times higher than

in other corrosion zones. Corrosion prevention techniques are now well-established in this zone [10], but the cleaning equipment for fouling organisms have yet to be improved. Research on underwater cleaning equipment has been carried out in some countries, but some still require the assistance of a diver to operate it [11,12]. Currently, the traditional manual cleaning method is still used in China, which has some drawbacks such as low cleaning efficiency, short operation window, weather influence, and difficult operation. Therefore, the problem of using mechanical equipment to automatically remove fouling organisms has not been resolved.

Most of the current research has focused on ship surface cleaning equipment such as the underwater cleaning equipment developed by the UMC Company in the UK [13]. The equipment generates negative pressure suction through a reverse rotating brush, thereby adsorbing and maintaining it on the surface of the ship; with the assistance of divers, the device can be equipped with four different types of rotary brushes such as silicone bristles (soft), polypropylene bristles (hard), nylon cleaning brushes, and steel wire brushes to clean media with different adhesion forces. Procurement customers can also selectively install metal scraper blades at the front to remove hard and upright fouling organisms, but the equipment still requires diver assistance. Nassiraei et al. [14] from the Kyushu University of Technology in Japan developed a type of wheeled hull surface cleaning equipment. This equipment was based on thrust adsorption technology and equipped with six suction thrusters and two rotating cleaning mechanisms; it can also be controlled remotely, and operators can observe the cleaned surface in real-time through their front and rear cameras as well as record and store images before and after cleaning. The cleaning equipment tested completed basic motion control tests and ship cleaning tests, and the reliability of the cleaning equipment was verified through tests. However, there was a deficiency as it requires divers to perform underwater auxiliary operations. Souto et al. [15,16], from the University of La Coruna in Spain, designed non-magnetic cleaning equipment for complex ship hull surfaces. This equipment adopted a hybrid technology of thrust and negative pressure adsorption and equipped with a rotary brush cleaning method. Two cleaning units can cross complex obstacles on the same surface or crawl from one surface to another surface that was perpendicular to it through a similar "walking" alternating adsorption method during the crawling process. Through the kinematics research, simulation analysis, and underwater hull surface cleaning test, the equipment achieved good test results, but the equipment moved and cleaned slowly.

Most of the cleaning equipment above-mentioned targets the surface of the ship, but there has been relatively little research on cleaning equipment used for offshore steel piles. For instance, the Australian Iasgroup Company [17,18] has developed two cleaning robots, Splash Genius and Splash Genius II, for the cleaning of marine infrastructure platforms. These two cleaning robots can automatically clean the marine infrastructure platforms. Splash Genius adopts the surrounding clamping and climbing technology, and is equipped with a high-pressure water jet to remove the fouling organisms attached to the marine steel piles. Splash Genius II is an upgraded product of Splash Genius, which realized various autonomous control methods based on Splash Genius, thus there are significant savings not only in terms of the labor costs and force, but could also improve the cleaning efficiency. However, there are situations where the high-pressure water jet is not thoroughly cleaned. Woolfrey's [19–21] team at the University of Technology Sydney, Australia developed the Submersible Pile Inspection Robot (SPIR), which is an underwater cleaning robot. SPIR adopts clamping arm and climbing technology equipped with a high-pressure water jet, and can clean cylindrical or square steel piles. However, the SPIR is larger in size and has higher manufacturing costs. From the perspective of the operation process, the cleaning effect was not significant. The domestic research carried out in the field of cleaning marine steel piles started relatively late. At press, some universities have carried out relevant research, for example, CNOOC Energy Development Co. Ltd. And Yang Canjun's team [22–24] at Zhejiang University developed a cleaning robot called "HOME". HOME is composed of a four-wheel permanent magnet adsorption module and passive roll joint, which ensures

the self-adaptive adjustment function. HOME adopted the cavitation jet cleaning method, which means that it can automatically clean the fouling organisms attached to the steel piles within 100 m below the water surface. A panoramic visual navigation system was applied to HOME, which can sense the real-time surrounding environment and cleaning status. However, there were some problems such as incomplete cleaning from the actual cleaning effect, which did not meet our requirements for the follow-up multiple layers of Petrolatum Tape Cover anticorrosion technology (PTC) [25] on steel piles. Wang Liquan's team [26,27] at Harbin Engineering University designed a cleaning robot for marine steel piles that adopted an upper and lower ring structure including upper and lower clamps. Three telescopic hydraulic cylinders were connected between the two ring structures as telescopic mechanisms, which could realize the telescopic crawling of the robot. A gear rotation structure was designed in the middle part to connect the scraping tools to ensure that the scraping tools could rotate at a certain angle in order to continue to clean vertically along the axis of the steel pile. However, the overall structure of the robot was relatively complex, which easily affected the cleaning speed and stability during the robot operation. At Shandong University, Yu Fujie et al. [28] designed an underwater cleaning robot with a manipulator for an offshore jacket called ROVMS. The ROVMS was used to generate the adsorption force through the electromagnetic adsorption unit, and the ROVMS could maintain its distance from the surface to be cleaned. Four rollers were designed for the ROVMS to realize its stable support and prevent its body from colliding with the steel pile in the contact direction of the cleaning surface. The ROVMS adopts the cavitation jet method and has the adaptability of resisting the interference of ocean current, but there is still the possibility of incomplete cleaning.

Currently, most marine steel pile cleaning equipment is equipped with a water jet cleaning method. In this paper, a configuration scheme of marine steel pile cleaning equipment by the scraping method and its telescopic mechanism is proposed by applying a multi-cylinder synchronous control strategy to cleaning equipment, which can effectively avoid the problem of cleaning equipment eccentricity and tilt. If the synchronization accuracy is too high, the control method will lead to an increase in manufacturing costs and unnecessary resource waste; if the synchronization accuracy is too low, it will cause asynchronous expansion and contraction during the operation of the telescopic mechanism, leading to eccentricity and tilt of the cleaning equipment, thereby affecting the cleaning effect of the scraping tools. Therefore, conducting research on the three-cylinder synchronous control method with a telescopic mechanism to ensure the synchronization of the cleaning equipment's telescopic mechanism operation and achieve the effective removal of attached marine fouling is of great significance for the development of marine steel pile cleaning equipment.

2. Cleaning Equipment Structure Scheme and Working Principle

Marine steel pile cleaning equipment is composed of the frame, clamps, hinges and locks, and scraping tools. The overall structure is shown in Figure 1. The frame includes upper and lower rings and telescopic mechanisms. The upper and lower rings are composed of two half rings that can be opened to encircle the steel piles. The cleaning equipment can be held on the steel pile by the clamps. The telescopic mechanism is composed of three telescopic hydraulic cylinders that are connected between the upper and lower ring platforms with bolts. It not only supports the upper and lower ring platforms, but also controls the distance between them. Through the telescopic mechanism of three hydraulic cylinders and the cooperation of two groups of clamps, the cleaning equipment can move along with the steel pile. The scraping tools are composed of four groups of blade, each group including a driven hydraulic cylinder and a scraping blade. The driven hydraulic cylinder drives the scraping blade to clean the attached fouling organisms along the marine steel pile at a certain angle through the telescopic mechanism. The opening and closing of the equipment's upper and lower half rings are controlled by the hinges and locks through the hydraulic cylinder.
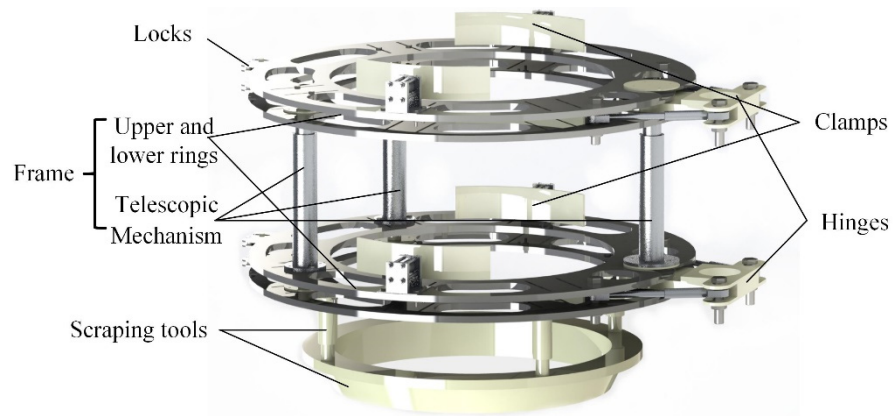
Figure 1. 3D model plan of the marine steel pile cleaning equipment.

The working area of the designed cleaning equipment is the spray splashing area or the tidal range area. Therefore, the equipment should be able to work on and under the water at the same time, and its working range is ±20 m above sea level. The fouling organisms attached to the marine steel piles in this area are relatively serious. The steel pile surface shall be treated as PTC after cleaning. The cleaning equipment designed at present can clean the marine steel piles with a diameter of 1 m. The creeping speed of the cleaning equipment along the axis of the marine steel pile is about 1 m/20 min to 1 m/30 min. The scraping tools are made of an aluminum alloy. In order to reduce the overall weight of the equipment, carbon fiber and aluminum alloy were used as the main frame materials.

With the assistance of the lifting boat, the staff installed the cleaning equipment on the marine steel piles with the upper and lower rings open. After installation, the equipment could automatically clean the marine steel piles. In the initial state, the cleaning equipment is clamped by the upper and lower clamps to hold the equipment onto the steel pile. In the climbing stage, when the equipment is ready to move downward, the lower clamps are released, and the hydraulic cylinder of the telescopic mechanism is extended simultaneously. When the hydraulic cylinder is extended to its limit, the lower clamps are clamped. At the end of climbing, the upper clamps are released, the telescopic mechanism is retracted to its limit, and the upper clamping hydraulic cylinder is clamped. At this time, the cleaning equipment completes its downward movement and moves to a new position on the steel pile. In the cleaning stage, two groups of clamps are clamped, and the scraping tools reciprocates vertically along the steel pile. By repeating the above steps, the steel piles in the entire splash zone can be cleaned. The schematic diagram of cleaning operation is shown in Figure 2.
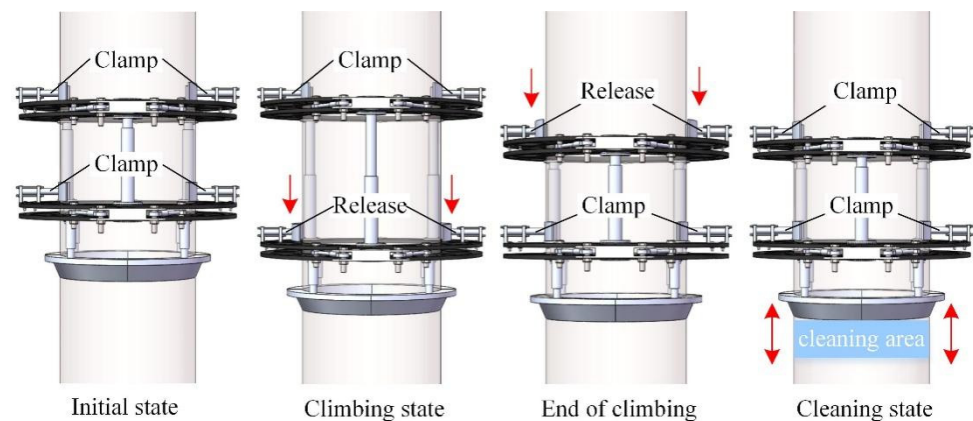
Figure 2. Operation process of the cleaning equipment (The red arrow indicates the direction of movement).

3. Influence of Telescopic Mechanism Synchronization on Scraping Tools

During the operation of the cleaning equipment in the ideal state, when the clamps clamp onto the marine steel pile, the upper and lower rings of the cleaning equipment should be kept horizontal, and the centers of the two rings and the steel pile should be concentric, as shown in Figure 3a, which is a top view of the cleaning equipment. When the center line of the upper and lower rings of the cleaning equipment (referred to as the cleaning equipment center line) coincides with the center line of the steel pile, the cleaning equipment is not inclined, as shown in Figure 3b, which is a cross-sectional view of the cleaning equipment. In this state, the angle of the blade is normal, the included angle between the blade and the steel pile is α_0, and the rake angle of the blade is $\gamma_0 = (90° - \alpha_0)$. Under the condition of no tilt, it is assumed that the cleaning equipment is ready to clean the annual barnacles that have attached to the circumference of the marine steel pile. According to the calculation, the four scraping tools of the cleaning equipment can be subjected to a total reaction force of about 6520 N when cleaning the attached barnacles [26].

(a)	**(b)**
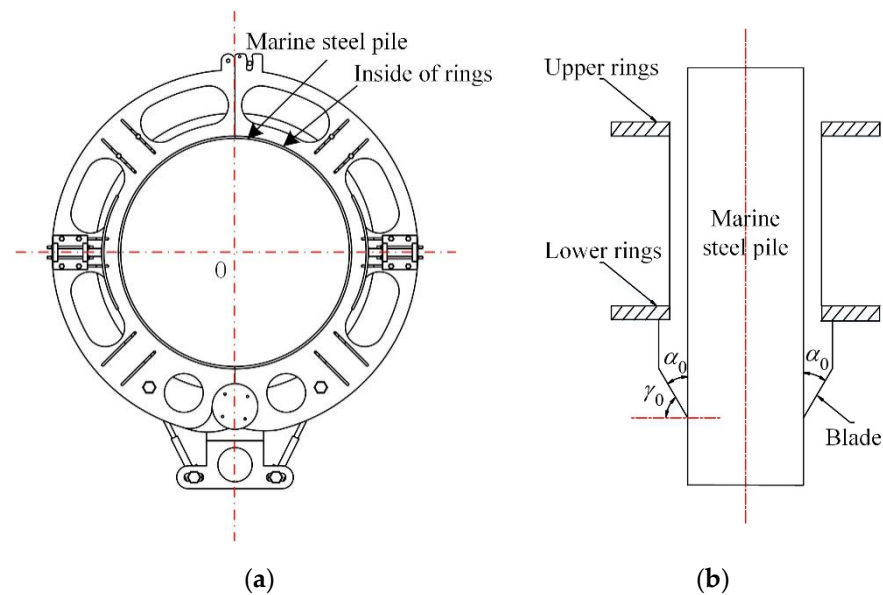
Figure 3. The working position of the cleaning equipment in an ideal state: (**a**) concentric; (**b**) no tilt.

During the operation of the cleaning equipment, due to the synchronization error of the telescopic mechanism, the eccentricity in or tilt of the cleaning equipment may occur as shown in Figure 4. Compared to Figure 3, when eccentric, as shown in Figure 4a, the included angle between the blade and the steel pile surface α_0 changed, so that the angle between the blade on one side and the steel pile was $\alpha_1 < \alpha_0$, and the angle between the opposite blade and steel pile was $\alpha_2 > \alpha_0$, which further caused the change in the rake angle of the blade and affected the cleaning effect of the cleaning equipment. When tilted, as shown in Figure 4b, the included angle of the blade close to the side of the steel pile was $\alpha_3 < \alpha_0$, and the angle between the opposite blade and steel pile was $\alpha_4 > \alpha_0$, which also affected the cleaning effect and the stability of the cleaning equipment. Next, the multi-cylinder synchronous control method was applied to the telescopic mechanism of the cleaning equipment for modeling and analysis.
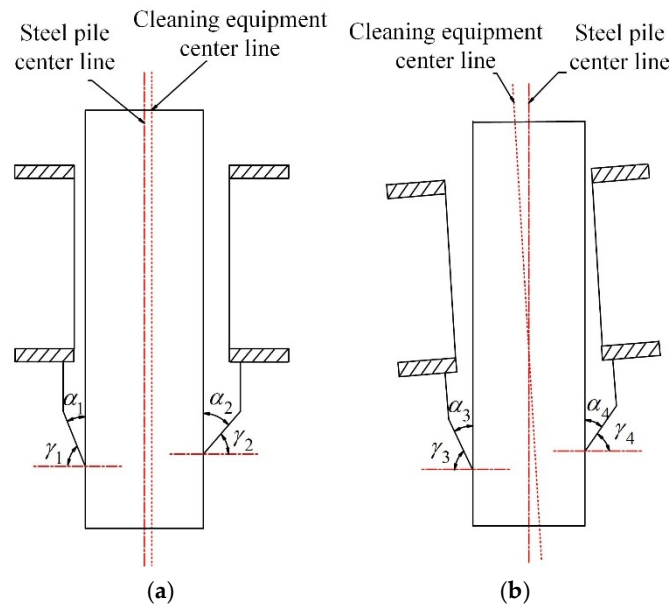
Figure 4. Operation process of cleaning equipment: (**a**) eccentricity of the cleaning equipment; (**b**) tilt of the cleaning equipment.

4. Synchronous Modeling and Simulation of the Telescopic Mechanism

4.1. Modeling of Synchronous Control System of the Telescopic Mechanism

The mathematical model of the synchronous extending process of the telescopic mechanism was established, as shown in Figure 5. The three hydraulic cylinders were connected by flanges. Each hydraulic cylinder could be rotated around the *x*-axis with a rotation angle of θ_{xi}, and around the *y*-axis with a rotation angle of θ_{yi}, where $I = 1, 2, 3$. In order to simplify the form of load motion, the following assumptions were made:

(1) Assuming that the piston of the hydraulic cylinder does not rotate in the cavity, there is no degree of freedom to twist around the *z*-axis for the telescopic load;

(2) Assuming that the synchronization error of the three-cylinder is much smaller than the distance between the installation positions of each hydraulic cylinder, the telescopic load mainly moves in the vertical direction, that is, the *z*-axis direction, and can be ignored along the *x*-axis and *y*-axis directions;

(3) Assuming that the hydraulic cylinder piston is not affected by the lateral force, regardless of the gravity of the piston and cylinder, the output force F_i ($I = 1, 2, 3$) of the piston rod of the hydraulic cylinder is along the direction of the piston rod, and the angle with the *z*-axis is approximately zero;

(4) Assume that the upper flange of the hydraulic cylinder and the upper ring are connected by a point centered on the flange.
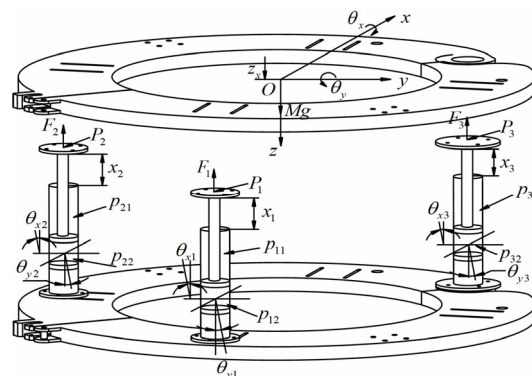
Figure 5. Operation process of the cleaning equipment.

On the basis of the above assumptions, the coordinate system of the system was established as follows:

In the figure, *O-xyz* is the model coordinate system, the center of mass of the above ring is the coordinate origin *O*, and the *x*, *y*, and *z* axes are as shown in Figure 5. In this way, the load movement such as the telescopic upper ring during the crawling process of the cleaning equipment can be simplified into three degrees of freedom: the degree of freedom of vertical motion in the *z*-axis direction, the degree of freedom of rotation around the *x*-axis, and the degree of freedom of rotation around the *y*-axis. That is to say, the movement of the telescopic load during the crawling process of the cleaning equipment can be described by the displacement z_c of the center of mass in the *z*-axis direction, the rotation angle θ_{xi} of the load around the *x*-axis, and the rotation angle θ_{yi} of the load around the *y*-axis.

4.1.1. Equation of Motion of Telescopic Mechanism

When the lower clamps of the cleaning equipment are clamped, the upper clamps are released, and the hydraulic cylinder of the telescopic mechanism is mainly extended. The above ring is the object of load research, which realizes the telescopic motion of the upper ring, the positive direction of each vector, and the force analysis results, as shown in Figure 5. On the three degrees of freedom of the hydraulic cylinder extending, using Newton's second law and the law of rigid body rotation, we obtain [29–31]:

$$\begin{cases} -\sum_{i=1}^{3} F_i + Mg = M\ddot{z}_x \\ -\sum_{i=1}^{3} F_i P_{iy} = J_x\ddot{\theta}_x \\ -\sum_{i=1}^{3} F_i P_{ix} = J_y\ddot{\theta}_y \end{cases} \tag{1}$$

where F_i is the output force of the *i-th* hydraulic cylinder piston, (N); M is the total mass of load, (kg); z_x is the displacement of the center of mass of the load in the *z*-axis direction, (m); P_{ix} is the coordinate component of the P_i point on the *x*-axis in the coordinate system, (m); P_{iy} is the coordinate component of the *y*-axis of the P_i point in the coordinate system, (m); J_x is the moment of inertia of the telescopic load to the *x*-axis, (kg·m²); J_y is the moment of inertia of the telescopic load to the *y*-axis, (kg·m²); θ_x is the angle of rotation of the telescopic load about the *x*-axis, (rad), which is positive in the counterclockwise direction along the *Ox*-axis; θ_y is the rotation angle of the telescopic load around the *y*-axis, (rad), which is positive in the counterclockwise direction along the *Oy*-axis.

4.1.2. Telescopic Load and Point Contact Position Equation of Hydraulic Cylinder

Consider that when the telescopic load makes a small rotation in the *O-xyz* coordinate system, the coordinate of any point P_i on the *z*-axis can be approximated by $(z_x, \theta_x, \theta_y)$ as:

$$P_{iz} = z_x + P_{iz0} + P_{iy}\theta_x + P_{ix}\theta_y \tag{2}$$

where P_{iz} is the coordinate component of the *z*-axis of the P_i point in the coordinate system *O-xyz*, (m); P_{iz0} is the coordinate component of the *z*-axis of the initial P_i point in the coordinate system *O-xyz*, (m); z_x is the displacement of the piston rod of the hydraulic cylinder, (m).

Therefore, the approximate expressions of the displacements of the three hydraulic cylinder pistons from Equation (2) can be obtained as:

$$x_i = P_{iz} - P_{iz0} = z_x + P_{iy}\theta_x + P_{ix}\theta_y \tag{3}$$

Select P_1, P_2, and P_3 to form a set of three points that are not on a straight line on the plane. Let P_1, P_2, and P_3 constitute the minimum point set of the telescopic load attitude.

Define $x_q = \begin{pmatrix} x_1 & x_2 & x_3 \end{pmatrix}^T$ as the displacement vector of the piston rod of each hydraulic cylinder, then x_q and $\begin{pmatrix} z_x & \theta_x & \theta_y \end{pmatrix}^T$ have the following relationship:

$$x_q = \begin{pmatrix} 1 & P_{1y} & P_{1x} \\ 1 & P_{2y} & P_{2x} \\ 1 & P_{3y} & P_{3x} \end{pmatrix} \begin{pmatrix} z_x \\ \theta_x \\ \theta_y \end{pmatrix} = L_q \begin{pmatrix} z_x \\ \theta_x \\ \theta_y \end{pmatrix} \tag{4}$$

4.1.3. The Equation of Motion of the Piston Rod of a Hydraulic Cylinder

Taking the piston rod of each hydraulic cylinder as the research object, its various vector directions and force results are shown in Figure 5. Considering that the hydraulic cylinder moves approximately vertically, Newton's second law is applied to the piston rod of the hydraulic cylinder in the vertical direction:

$$\begin{cases} p_{iL}A_{i1} + F_i + m_i g - B_{ip}\dot{x}_i = m_i \ddot{x}_i \\ p_{iL} = p_{i1} - p_{i2}A_{i2}/A_{i1} \end{cases} \tag{5}$$

where p_{iL} is the load pressure of the *i-th* hydraulic cylinder, (Pa); p_{iL} is the rodless chamber pressure of the *i-th* hydraulic cylinder, (Pa); p_{i2} is the rod chamber pressure of the *i-th* hydraulic cylinder, (Pa); A_{i1} is the rodless cavity area of the *i-th* hydraulic cylinder, (m); A_{i2} is the rod cavity area of the *i-th* hydraulic cylinder, (m); m_i is the rod cavity area of the *i-th* hydraulic cylinder, (m); B_{ip} is the viscous damping coefficient of the *i-th* hydraulic cylinder, (N·s/m).

4.1.4. Load Pressure Dynamic Characteristic Equation of Asymmetric Hydraulic Cylinder

Since the three-cylinder drive system in the model adopts the form of one-to-one valve-controlled cylinders, the oil flow into each hydraulic cylinder is controlled by its own proportional valve. The dynamic characteristics of the load pressure in the *i-th* hydraulic cylinder can be expressed by the following equation:

$$\begin{cases} \dot{p}_{iL} = \dfrac{\beta_e}{V_{ie}(x_i)} \left[Q_{iL}(x_{iv}, p_{iL}) - C_{it}p_{iL} - A_{i1}\dot{x}_i \right] \\[2mm] V_{ie}(x_i) = \dfrac{A_{i1}(S_i + 3x_i)}{7.5} \\[2mm] C_{it} = \dfrac{1.5C_{ip} + C_{ep}}{1.25} \end{cases} \tag{6}$$

where p_{iL} is the load pressure of the *i-th* hydraulic cylinder, (Pa); V_{ie} is the equivalent volume of the *i-th* hydraulic cylinder, (m³); β_e is the oil modulus of elasticity, Pa; Q_{iL} is the load flow of the *i-th* valve, (m³/s); x_{iv} is the displacement control signal of the *i-th* valve, (m); A_{i1} is the rodless cavity area of the *i-th* hydraulic cylinder, (m); S_i is the total stroke of the *i-th* hydraulic cylinder, (m); C_{it} is the total leakage coefficient of the *i-th* hydraulic cylinder, (m⁵/N·s); C_{ip} is the internal leakage coefficient of the *i-th* hydraulic cylinder, (m⁵/N·s); C_{ep} is the external leakage coefficient of the *i-th* hydraulic cylinder, (m⁵/N·s);

4.1.5. Mathematical Model of Three-Cylinder System

The three-cylinder system can be described according to Equations (4)–(6). Defining $F = \begin{pmatrix} F_1 & F_2 & F_3 \end{pmatrix}^T$ as the force vector of the load acting on the P_i contact point, Equations (1) and (5) can be arranged as:

$$\begin{cases} -L_f F + Mg = M_L \ddot{x}_q \\ R - B_p \dot{x} + F = m\ddot{x} \end{cases} \tag{7}$$

In the formula, $L_f = \begin{pmatrix} 1 & 1 & 1 \\ P_{1y} & P_{2y} & P_{3y} \\ P_{1x} & P_{2x} & P_{3x} \end{pmatrix}$ is the arm matrix of the force F; $M_g = \begin{pmatrix} M_g \\ 0 \\ 0 \end{pmatrix}$
is the gravity matrix of the telescopic load; $M_L = diag(M \quad J_x \quad J_y)L_q^{-1}$ is the inertia matrix
of the telescopic load; $R = \begin{pmatrix} p_{1L}A_{11} + m_1 g \\ p_{2L}A_{21} + m_2 g \\ p_{3L}A_{31} + m_3 g \end{pmatrix}$ is the hydraulic cylinder load resultant exter-
nal force matrix; $B_p = diag(B_{1p} \quad B_{2p} \quad B_{3p})$ is the matrix of viscous damping coefficient
of hydraulic cylinder piston; $m = diag(m_1 \quad m_2 \quad m_3)$ is the mass matrix of the hydraulic
cylinder piston.

Equation (7), after eliminating F, obtains the motion equation of the telescopic
load, namely:

$$(M_L + L_f m)\ddot{x}_q + L_f B_p \dot{x}_q = L_f \tau \tag{8}$$

In the formula, $\tau = L_f^+ M_g + R$, L_f^+ is the generalized inverse of L_f.

Let $M_{xq} = M_L + L_f m$, $B_{xp} = L_f B_p$, the mathematical model of the three-cylinder
system can be obtained by combining Equations (6) and (8), namely:

$$\begin{cases} M_{xq}\ddot{x} + B_{xp}\dot{x}_q = L_f \tau \\ \dot{p}_{iL} = \beta_e K_{iq}\psi_i(x_i, p_{iL})x_{iv} + \pi(x_i)p_{iL} + h_i(x_i)\dot{x}_i \end{cases} \tag{9}$$

In the formula, $K_{iq} = C_d \omega_1$, $h(x_i) = \frac{\beta_e A_{i1}}{V_{ie}(x_i)}$.

Among them, C_d is the valve port flow coefficient; ω_1 is the area gradient of valve
port, (m^2/m).

In the formula, $\psi(x_i) = \frac{1}{V_{ie}(x_i)}\sqrt{\frac{4\alpha_{XV}p_s - \frac{x_{iv}}{|x_{iv}|}p_{iL}}{3\rho}}$, $\pi(x_i) = -\frac{C_{it}\beta_e}{V_{ie}(x_i)}$.

Among them, α_{XV} is the commutation factor of the valve, when $x_v > 0$, $\alpha_{XV} = 1$,
when $x_v < 0$, $\alpha_{XV} = \eta$, $\eta = A_{i2}/A_{i1}$; ρ is the density of oil, (kg/m^3), for Equation (9), when
$L_f = \begin{pmatrix} 1 & 1 & 1 \\ P_{1y} & P_{2y} & P_{3y} \\ P_{1x} & P_{2x} & P_{3x} \end{pmatrix}$, $L_q = \begin{pmatrix} 1 & P_{1y} & P_{1x} \\ 1 & P_{2y} & P_{2x} \\ 1 & P_{3y} & P_{3x} \end{pmatrix}$ is taken, which is the mathematical model
of the three-cylinder system at this time. At this time, the expressions of M_{xq}, B_{xp}, and τ are:

$$M_{xq} = M_L + L_f m =$$

$$\begin{pmatrix} m_1 + \dfrac{M(P_{2x}P_{3y} - P_{3x}P_{2y})}{P_{1x}P_{2y} - P_{2x}P_{1y} - P_{1x}P_{3y} + P_{3x}P_{1y} + P_{2x}P_{3y} - P_{3x}P_{2y}} & \\ \dfrac{-J_x(P_{2x} - P_{3x})}{P_{1x}P_{2y} - P_{2x}P_{1y} - P_{1x}P_{3y} + P_{3x}P_{1y} + P_{2x}P_{3y} - P_{3x}P_{2y}} & \\ \dfrac{J_y(P_{2y} - P_{3y})}{P_{1x}P_{2y} - P_{2x}P_{1y} - P_{1x}P_{3y} + P_{3x}P_{1y} + P_{2x}P_{3y} - P_{3x}P_{2y}} & \\[2em] \dfrac{-M(P_{1x}P_{3y} - P_{3x}P_{1y})}{P_{1x}P_{2y} - P_{2x}P_{1y} - P_{1x}P_{3y} + P_{3x}P_{1y} + P_{2x}P_{3y} - P_{3x}P_{2y}} & \\ m_2 P_{2y} + \dfrac{J_x(P_{1x} - P_{3x})}{P_{1x}P_{2y} - P_{2x}P_{1y} - P_{1x}P_{3y} + P_{3x}P_{1y} + P_{2x}P_{3y} - P_{3x}P_{2y}} & \\ \dfrac{-J_y(P_{1y} - P_{3y})}{P_{1x}P_{2y} - P_{2x}P_{1y} - P_{1x}P_{3y} + P_{3x}P_{1y} + P_{2x}P_{3y} - P_{3x}P_{2y}} & \\[2em] \dfrac{M(P_{1x}P_{2y} - P_{2x}P_{1y})}{P_{1x}P_{2y} - P_{2x}P_{1y} - P_{1x}P_{3y} + P_{3x}P_{1y} + P_{2x}P_{3y} - P_{3x}P_{2y}} & \\ \dfrac{-J_x(P_{1x} - P_{2x})}{P_{1x}P_{2y} - P_{2x}P_{1y} - P_{1x}P_{3y} + P_{3x}P_{1y} + P_{2x}P_{3y} - P_{3x}P_{2y}} & \\ m_3 P_{3x} + \dfrac{J_y(P_{1y} - P_{2y})}{P_{1x}P_{2y} - P_{2x}P_{1y} - P_{1x}P_{3y} + P_{3x}P_{1y} + P_{2x}P_{3y} - P_{3x}P_{2y}} & \end{pmatrix} \tag{10}$$

$$B_{xp} = L_f \cdot diag \begin{pmatrix} B_{1p} & B_{2p} & B_{3p} \end{pmatrix} \tag{11}$$

$$\tau = \begin{pmatrix} A_{11}p_{1L} + m_1 g + \dfrac{M_g \left(P_{2x}P_{3y} - P_{3x}P_{2y} \right)}{P_{1x}P_{2y} - P_{2x}P_{1y} - P_{1x}P_{3y} + P_{3x}P_{1y} + P_{2x}P_{3y} - P_{3x}P_{2y}} \\[3ex] A_{21}p_{2L} + m_2 g - \dfrac{M_g \left(P_{1x}P_{3y} - P_{3x}P_{1y} \right)}{P_{1x}P_{2y} - P_{2x}P_{1y} - P_{1x}P_{3y} + P_{3x}P_{1y} + P_{2x}P_{3y} - P_{3x}P_{2y}} \\[3ex] A_{31}p_{3L} + m_3 g + \dfrac{M_g \left(P_{1x}P_{2y} - P_{2x}P_{1y} \right)}{P_{1x}P_{2y} - P_{2x}P_{1y} - P_{1x}P_{3y} + P_{3x}P_{1y} + P_{2x}P_{3y} - P_{3x}P_{2y}} \end{pmatrix} \tag{12}$$

4.2. Synchronous Control Simulation of Telescopic Mechanism

Based on the above theoretical analysis, the operation simulation model of the telescopic mechanism driven by three cylinders was established including three-channel load coupling modules and three single-channel electro-hydraulic servo drive modules. The single channel electro-hydraulic servo drive module includes a PID controller, proportional valve module, valve control cylinder load flow module, flow continuity module, and hydraulic cylinder piston dynamic characteristics module. Using the basic modules provided in MATLAB Simulink in the subsystem mode, the classic PID simulation model of the three-cylinder telescopic drive system was established. The established simulation model of the three-cylinder telescopic drive system is shown in Figure 6.

Figure 6. Synchronous telescopic system of three hydraulic cylinders.

According to the Simulink simulation model of the three-cylinder system obtained from the above analysis, the specific simulation experiments were carried out as follows: during the simulation, the hydraulic cylinder accelerated for 0.5 s to reach the working speed of 100 mm/s, and then moved at the working speed, with the maximum working stroke of 500 mm, and the simulation running time of 10 s.

Based on the analysis of the working principle of the marine steel pile cleaning equipment, it can be seen that the three-cylinder drive system had three typical working conditions: the no-load operation of the telescopic mechanism, the operation of the telescopic mechanism under the scraping reaction load, and the operation of a single hydraulic cylinder under the scraping reaction load. The displacement synchronization error curve of the three-cylinder was obtained, as shown in Figure 7.
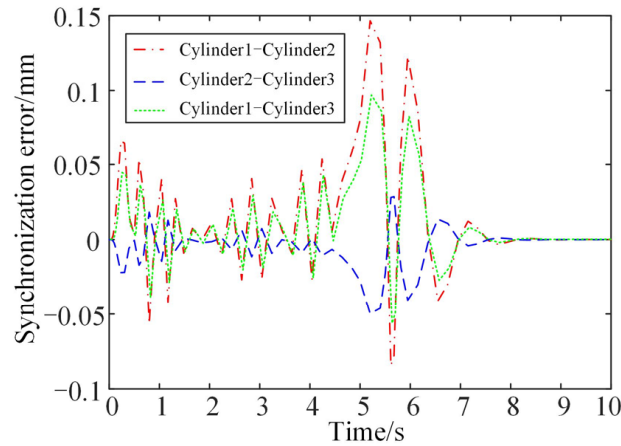
(**a**)
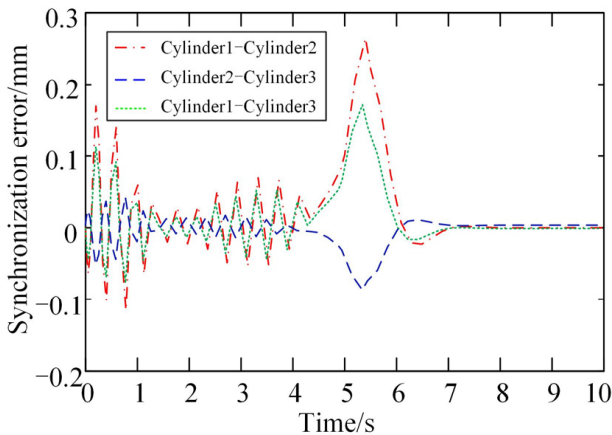
(**b**)
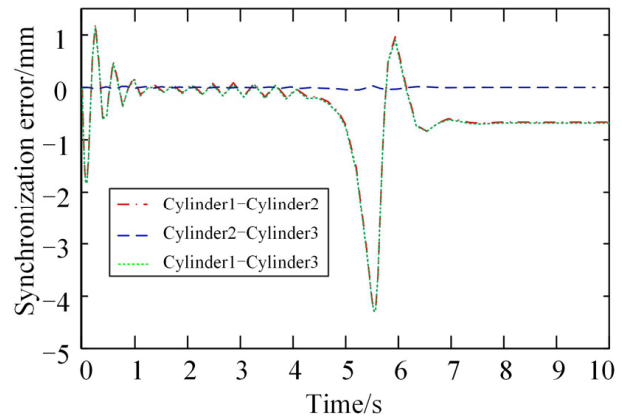
(**c**)

Figure 7. Three-cylinder synchronization error tracking simulation curve: (**a**) no-load operation of the telescopic mechanism; (**b**) the operation of the telescopic mechanism under the scraping reaction load; (**c**) the operation of a single hydraulic cylinder under the scraping reaction load.

Under the no-load condition of the telescopic mechanism, it can be seen from the displacement synchronization error curve of the three cylinders in Figure 7a that when the 0.5 s hydraulic cylinder started, the fluctuation of the synchronization error tracking curve between each cylinder started to increase, and the maximum error of the two cylinders was about 0.05 mm. During the hydraulic cylinder extending process, the synchronization error between the two cylinders was relatively small, which was kept at about 0.05 mm. When the hydraulic cylinder stopped extending from 4 s to 8 s, and was about to reach the limit displacement of 500 mm, the piston entered the deceleration stage, the displacement synchronization error curve between each cylinder fluctuated most obviously, and the maximum synchronization error of cylinder 1 and cylinder 2 was about 0.15 mm, the maximum synchronization error of cylinder 1 and cylinder 3 was about 0.1 mm, the

maximum synchronization error of cylinder 2 and cylinder 3 was about 0.025 mm; the synchronous error tracking curve between each cylinder was basically stable during the operation stage. When the extending limit position was reached, the displacement error between each cylinder was finally maintained at 0 mm.

Under the loaded condition of the telescopic mechanism by the scraping reaction force, it can be seen from the displacement synchronization error curve of the three cylinders in Figure 7b that when the 0.5 s hydraulic cylinder started, the fluctuation of the synchronization error tracking curve between each cylinder started to increase, and the maximum error of the two cylinders was about 0.15 mm. During the hydraulic cylinder extending process, the synchronization error between the two cylinders was relatively small, and the synchronization error was kept at about 0.05 mm. When the hydraulic cylinder stopped extending from 4 s to 8 s, and was about to reach the limit displacement of the 500 mm waiting position, the piston entered the deceleration stage, the displacement synchronization error curve between each cylinder fluctuated most obviously, and the maximum synchronization error of cylinder 1 and cylinder 2 was about 0.28 mm, the maximum synchronization error of cylinder 1 and cylinder 3 was about 0.18 mm, the maximum synchronization error of cylinder 2 and cylinder 3 was about 0.1 mm; the synchronous error tracking curve between each cylinder was basically stable during the operation stage. When the extending limit position was reached, the displacement error between each cylinder was finally maintained at 0 mm.

Under the condition that a single hydraulic cylinder (hydraulic cylinder 1) is loaded with the scraping reaction force, it can be seen from the displacement synchronization error curve of three cylinders in Figure 7c that the synchronization error between cylinder 2, cylinder 3 and cylinder 1 was relatively large and the synchronization error between cylinder 2 and cylinder 3 was almost zero. When the hydraulic cylinder started, the synchronous error tracking curve fluctuation between cylinder 2 and cylinder 3 started to increase, and the maximum error of the two cylinders was about 1.8 mm. During the hydraulic cylinder extending process, the synchronization error between the two cylinders was relatively small, and the synchronization error was maintained at about 0.05 mm; When the hydraulic cylinder stopped extending from 4 s to 8 s, and was about to reach the limit displacement of 500 mm, the piston entered the deceleration stage, the displacement synchronization error curve between each cylinder fluctuated most obviously, and the maximum synchronization error between cylinder 2, cylinder 3, and cylinder 1 was about 4 mm, the synchronization error of cylinder 2 and cylinder 3 was about 0 mm; the synchronization error tracking curve between each cylinder was basically stable in the operation stage. When the extending limit position was reached, there was a 1 mm synchronization error between cylinder 2, cylinder 3, and cylinder 1, and the displacement error between cylinder 2 and cylinder 3 was finally maintained at 0 mm.

It can be seen from the above analysis that In the three cases, the synchronous error of the multi-cylinder displacement was small during the operation of the telescopic mechanism, and good synchronization could be achieved, which not only effectively guarantees the stability of the cleaning operation of the cleaning equipment, but also avoids the eccentricity and tilt of the cleaning equipment during the climbing and cleaning process.

5. Synchronous Test of the Telescopic Mechanism

5.1. Development and Test of Cleaning Equipment

Based on the design scheme and simulation results of the marine steel pile cleaning equipment proposed in this paper, a multi-cylinder driving telescopic mechanism test prototype was developed. During the manufacturing and processing of the test prototype, the working principle and system composition of the pneumatic transmission and hydraulic transmission were similar, and both could achieve the purpose of cleaning the climbing, so a cylinder with a relatively low economic cost was selected to replace the hydraulic cylinder in this design scheme to achieve the same effect. Although the air was compressible, the action speed of the cylinder was easily affected by the load, and the stability was not as

good as that of the hydraulic transmission [32]. If the cylinder can achieve the test effect stably, it would be even better when the hydraulic cylinder with better stability and more accurate control is used.

After assembling the clamps, telescopic mechanism, and scraping tools, the final developed cleaning equipment test prototype was obtained, as shown in Figure 8. In order to make its placement stable, the whole equipment was inverted, the scraping tools were located at the top, and the whole equipment was placed on the ground.

Figure 8. Cleaning equipment test prototype.

In order to verify the synchronization effect of simulation when the telescopic mechanism was under no-load, the telescopic mechanism was equipped with their respective displacement sensors, as shown in Figure 9a.

(**a**)

(**b**)
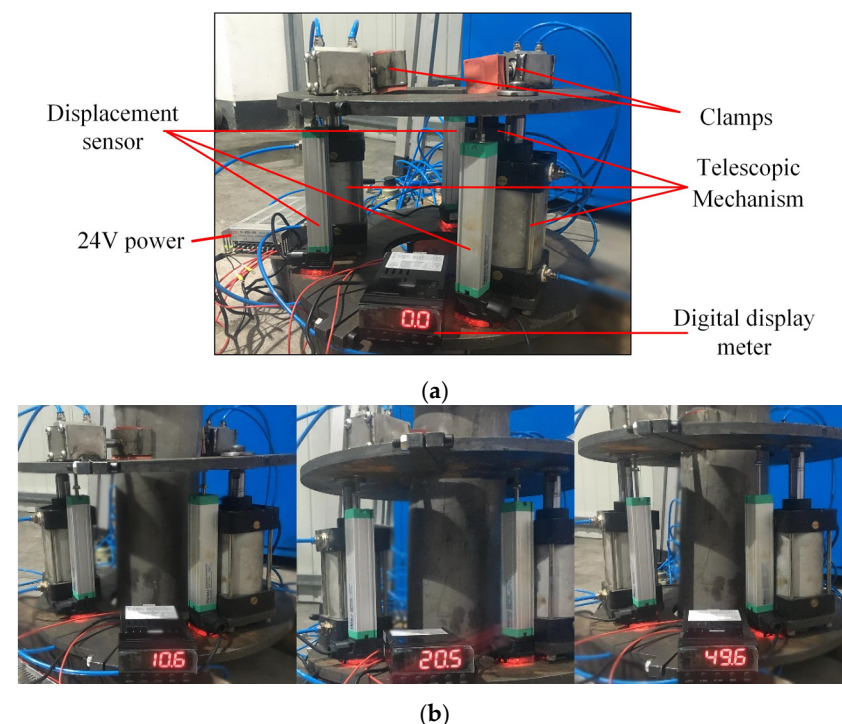
Figure 9. Three-cylinder synchronous test device diagram: (**a**) three-cylinder synchronous test device; (**b**) three-cylinder synchronous test.

The displacement sensor was fixed on the upper and lower support rings of the cleaning equipment to monitor the telescopic displacement of each cylinder in real-time. The three displacement sensors were connected to their respective digital display meters, and the telescopic displacement of each sensor can be fed back in real-time through the readings of their digital displays.

During the test, the clamps and telescopic mechanism switch of the cleaning equipment were operated through the console. The extending process of the three cylinders was monitored in real-time through the displacement sensor to carry out the telescopic synchronization test on the cleaning equipment.

In this test, the cleaning equipment prototype was produced with the telescopic mechanism gradually extending to its extreme position under the clamping state of the lower clamps, and the cleaning equipment was in an upward creeping state for testing. The test steps were as follows:

First, we controlled the lower clamps of the cleaning equipment to clamp and the upper clamps to release, so that the cleaning equipment was in the clamping state and stable on the steel pile; second, we ensured that the telescopic mechanism gradually extended, and the cleaning equipment started to climb up along the axis of the steel pile. During the climbing process, we monitored the extending displacement of the three cylinders in real-time, as shown in Figure 9b, took one cylinder as an example, and recorded the extending displacement data of the other two cylinders in the same way. Finally, when the telescopic mechanism reached its limit, the upper clamps clamped, and the upper and lower clamps were in the clamping state. This means that the cleaning equipment has completed an upward climbing movement along the axial direction of the steel pile, so the cleaning equipment can move up or down along the axial direction of the steel pile.

5.2. Test Results and Discussion

According to the synchronous displacement data of three cylinders, the extending displacement curve of three cylinders can be drawn under the same coordinate, as shown in Figure 10.
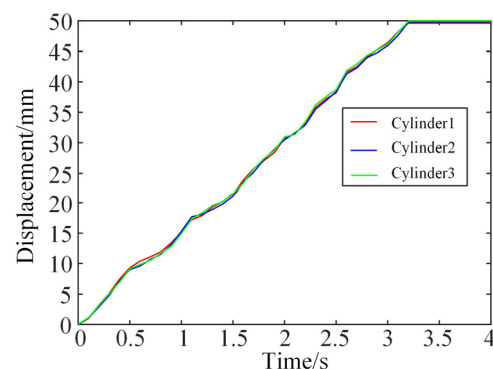
Figure 10. Synchronous displacement curve of the three-cylinder test.

It can be seen from Figure 10 that the displacement curve fluctuated slightly during the extending of the three cylinders, but the synchronization was good. The three cylinders almost reached the 50 mm position at the same time. After reaching this position, although the displacement of the three cylinders remained stable with the increase in time, the three hydraulic cylinders moved 49.6 mm, 49.8 mm, and 49.9 mm, with relative errors of 0.8%, 0.4%, and 0.2%, respectively. According to the data recorded by the displacement sensor, we depicted the error curve of the relative target displacement between each cylinder, as shown in Figure 11.

It can be seen from Figure 11 that the maximum displacement synchronization error of the cylinder 1 and cylinder 2 test reached 0.7 mm, the cylinder 2 and cylinder 3 test reached 0.7 mm, and the cylinder 1 and cylinder 3 test reached 0.6 mm. According to the test, the maximum displacement error between two different cylinders was controlled at 0.7 mm, the minimum displacement error was 0.1 mm, and the synchronous displacement error between the three cylinders was well controlled.
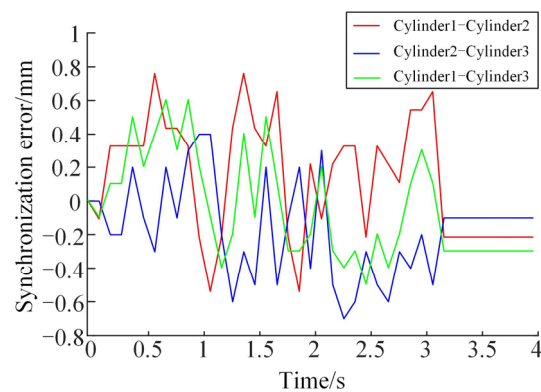
Figure 11. The three-cylinder test displacement synchronization error.

To sum up, when the extension of the telescopic mechanism reached the limit position of 50 mm, the relative error between the three cylinders and the target displacement was 0.8%, 0.4%, and 0.2%, respectively, to ensure that the equipment reached the specified working position at the given working speed. At the same time, the maximum error between the two cylinders was 0.7 mm, which effectively controlled the synchronization error between the two cylinders, and the synchronization of the telescopic mechanism was preliminarily verified.

6. Conclusions

In this paper, a configuration scheme of marine steel pile cleaning equipment and its telescopic mechanism with a multi-cylinder synchronous control strategy was proposed. Based on the MATLAB Simulink module, a simulation model of the operation process of the marine steel pile cleaning equipment was established, and its multi-cylinder synchronous control performance evaluation under multiple working conditions completed. The synchronous working performance of the telescopic mechanism of the cleaning equipment under no-load conditions was preliminarily verified through the test, and the following conclusions were obtained:

(1) In order to clean up the fouling organisms attached to the offshore infrastructure, this paper designed a new configuration of marine steel pile cleaning equipment using the scraping method and its telescopic mechanism with a multi-cylinder synchronous control strategy and process and produced a test prototype.

(2) The simulation model of the operation process of the marine steel pile cleaning equipment was established, and the simulation of its multi-cylinder synchronous control under multiple working conditions was completed. Through the simulation solution, the maximum displacement synchronization error between each cylinder of the telescopic mechanism under the no-load condition was 0.15 mm. When the three hydraulic cylinders were loaded by the scraping reaction force, the maximum synchronization error between each cylinder was about 0.28 mm; when a single hydraulic cylinder was loaded with the scraping reaction force, the maximum synchronization error between each cylinder was about 4 mm. In all three cases, the telescopic mechanism achieved good synchronization in the simulation process.

(3) Through the no-load test of the telescopic mechanism, the synchronization of the telescopic mechanism of the prototype of the cleaning equipment was preliminarily verified. The test results showed that the relative errors between the three cylinders and the target displacement were 0.8%, 0.4%, and 0.2%, respectively, to ensure that the equipment reached the designated working position at the given working speed. The displacement synchronization error of each cylinder was controlled within 1 mm, and the telescopic mechanism had good telescopic synchronization, which can prevent the eccentricity and tilt of the cleaning equipment during its operation while ensuring its stability.

References

1. Hopkins, G.; Davidson, I.; Georgiades, E.; Floerl, O.; Morrisey, D.; Cahill, P. Managing biofouling on submerged static artificial structures in the marine environment–assessment of current and emerging approaches. *Front. Mar. Sci.* **2021**, *8*, 759194. [CrossRef]
2. Azis, P.K.A.; Al-Tisan, I.; Al-Daili, M.; Green, T.N.; Ba-Mardouf, K.; Al-Qahtani, S.A.; Al-Sabai, K. Marine macrofouling: A review of control technology in the context of an on-line experiment in the turbine condenser water box of Al-Jubail Phase-I power MSF plants. *Desalination* **2003**, *154*, 277–290. [CrossRef]
3. Magin, C.M.; Cooper, S.P.; Brennan, A.B. Non-toxic antifouling strategies. *Mater. Today* **2010**, *13*, 36–44. [CrossRef]
4. Yebra, D.M.; Kiil, S.; Dam-Johansen, K. Antifouling technology—Past, present and future steps towards efficient and environmentally friendly antifouling coatings. *Prog. Org. Coat.* **2004**, *50*, 75–104. [CrossRef]
5. Ren, W.; Chen, Y.; Xv, H.; Chen, Y.; Xie, Z.; Chen, Y. Study of Corrosion Mechanism and Corrosion Status of Offshore Wind Power Equipment. *Ship Eng.* **2021**, *43*, 1–5.
6. Telegdi, J.; Trif, L.; Románszki, L. Smart anti-biofouling composite coatings for naval Applications. In *Smart Composite Coatings and Membranes*; Woodhead Publishing: Cambridge, UK; Elsevier: Amsterdam, The Netherlands, 2016; pp. 123–155.
7. Zan, Y.; Guo, R.; Yuan, L.; Ma, Q.; Zhou, A.; Wu, Z. Experimental study of a suspended subsea module at different positions in the splash zone. *Mar. Struct.* **2021**, *77*, 102935. [CrossRef]
8. Heaf, N.J. The Effect of Marine Growth On The Performance of Fixed Offshore Platforms in the North Sea. In Proceedings of the 11th Annual Offshore Technology Conference, Houston, TX, USA, 30 April–3 May 1979; pp. 255–267.
9. Campos, R.M.; Islam, H.; Ferreira, T.R.S.; Soares, C.G. Impact of heavy biofouling on a nearshore heave-pitch-roll wave buoy performance. *Appl. Ocean Res.* **2020**, *107*, 102500. [CrossRef]
10. Wei, S.C.; Xu, B.S.; Liang, X.B.; Wang, Y.J.; Liu, Y. Research on Corrosion-Resistance of High Velocity Arc Spray Coatings on Surface of Steel Structure in Splash Zone Environment. *Mater. Sci. Forum* **2011**, *675–677*, 1291–1294.
11. Albitar, H.; Dandan, K.; Ananiev, A.; Kalaykov, I. Underwater robotics: Surface cleaning technics, adhesion and locomotion systems. *Int. J. Adv. Robot. Syst.* **2016**, *13*, 7. [CrossRef]
12. Song, C.; Cui, W. Review of underwater ship hull cleaning technologies. *J. Mar. Sci. Appl.* **2020**, *19*, 415–429. [CrossRef]
13. Morrisey, D.; Woods, C. *In-Water Cleaning Technologies: Review of Information*; Ministry for Primary Industries, Manatū Ahu Matua: Wellington, New Zealand, 2015.
14. Nassiraei, A.A.F.; Sonoda, T.; Ishii, K. Development of ship hull cleaning underwater robot. In Proceedings of the 2012 Fifth International Conference on Emerging Trends in Engineering and Technology, Himeji, Japan, 5–7 November 2012; pp. 157–162.
15. Souto, D.; Faíña, A.; López-Peña, F.; Duro, R.J. Morphologically intelligent underactuated robot for underwater hull cleaning. In Proceedings of the 2015 IEEE 8th International Conference on Intelligent Data Acquisition and Advanced Computing Systems: Technology and Applications (IDAACS), Warsaw, Poland, 24–26 September 2015; pp. 879–886.
16. Souto, D.; Faíña, A.; López-Peña, F.; Duro, R.J. Lappa: A new type of robot for underwater non-magnetic and complex hull cleaning. In Proceedings of the 2013 IEEE International Conference on Robotics and Automation, Karlsruhe, Germany, 6–10 May 2013; pp. 3409–3414.
17. Iasgroup Corporation. Splash Genius II Cleaning System. Available online: http://www.ias-group.com.au/view/video-articles/splash-genius-ii-remotely-operated-cleaning-tool (accessed on 12 February 2023).
18. Iasgroup Corporation. Splash Genius Cleaning System. Available online: http://www.ias-group.com.au/view/video-articles/splash-genius-cleaning-tool (accessed on 12 February 2023).

19. Woolfrey, J.; Lu, W.; Vidal-Calleja, T.; Liu, D.J.O.E. Clarifying clairvoyance: Analysis of forecasting models for near-sinusoidal periodic motion as applied to AUVs in shallow bathymetry. *Ocean. Eng.* **2019**, *190*, 106385. [CrossRef]
20. Le, K.; To, A.; Leighton, B.; Hassan, M.; Liu, D. The spir: An autonomous underwater robot for bridge pile cleaning and condition assessment. In Proceedings of the 2020 IEEE/RSJ International Conference on Intelligent Robots and Systems (IROS), Las Vegas, NV, USA, 24 October 2020–24 January 2021; pp. 1725–1731.
21. Submersible Pile Inspection Robot. Available online: https://www.youtube.com/watch?v=hFtW2cXaHYk&t=24s (accessed on 12 February 2023).
22. Fan, J.; Yang, C.; Chen, Y.; Wang, H.; Huang, Z.; Shou, Z.; Jiang, P.; Wei, Q. An underwater robot with self-adaption mechanism for cleaning steel pipes with variable diameters. *Ind. Robot: Int. J.* **2018**, *42*, 193–205. [CrossRef]
23. Huang, Z.; Chen, Y.; Yang, C.; Fan, J.; Jiang, P. Teleoperate system of underwater cleaning robot based on HUD. In Proceedings of the 2017 11th Asian Control Conference (ASCC), Gold Coast, Australia, 17–20 December 2017; pp. 2675–2679.
24. Jiang, P.; Wei, Q.; Chen, Y.; Yang, C.; Fan, J.; Shou, Z.; Huang, Z. Real-time panoramic system for underwater cleaning robot. In Proceedings of the 2018 IEEE 9th International Conference on Mechanical and Intelligent Manufacturing Technologies (ICMIMT), Cape Town, South Africa, 10–13 February 2018; pp. 155–159.
25. Jie, P.; Baorong, H.; Jiali, L.; Weiguo, Z. Advance in application of petrolatum tape cover anticorrsion technology in China. *Corros. Prot.* **2015**, *36*, 1170–1173.
26. Chao, L.; Gang, W.; Chen, K.; Peng, J.; Liquan, W.; Xiangyu, W.; Feihong, Y. Analysis of removing barnacles attached on rough substrate with cleaning robot. *J. Mar. Sci. Eng.* **2020**, *8*, 569. [CrossRef]
27. Liquan, W.; Chao, L.; Kaiyun, C.; Gang, W. Mechanical research on removing adhesion barnacles with a cleaning robot for marine steel piles. *J. Harbin Eng. Univ.* **2021**, *42*, 259–265.
28. Fujie, Y.; Qingzhong, L.; Yao, W.; Yuan, C. Optimization of tool orientation for improving the cleaning efficiency of offshore jacket-cleaning systems. *Appl. Ocean Res.* **2021**, *112*, 102687.
29. Mo, W.; Liu, N.; Li, L.; Han, H. Application of PID control in hydraulic synchronous system of cleaning equipment. In *Journal of Physics: Conference Series*; IOP Publishing: Bristol, UK, 2021; pp. 62–64.
30. Kim, G.S.; Lee, D.J. Study on Optimization of Valve Parameter for Multi-Cylinder Synchronous Control System. *Adv. Sci. Lett.* **2015**, *21*, 2985–2988. [CrossRef]
31. Jing, N.; Hongliang, W.; Zhen, M.; Xiangqi, L. DCAT-NDI Control on Synchro-motion System with Multi-cylinder. *J. Hangzhou Dianzi Univ. Nat. Sci.* **2015**, *35*, 14–22.
32. Xiaoyao, Z.; Tao, W.; Bo, W. Synchronization Control of a 3-DOF Pneumatic Translational Parallel Robot. *Chin. Hydraul. Pneum.* **2021**, *45*, 129–134.